Ultraviolet−Visible Absorption Cross Sections of Gaseous HOI and Its Photolysis at 355 nm

Dieter Bauer, Trevor Ingham, Shaun A. Carl, Geert K. Moortgat, and John N. Crowley*

Max-Planck-Institut für Chemie, Division of Atmospheric Chemistry, Postfach 3060, 55020 Mainz, Germany

Received: December 5, 1997; In Final Form: February 4, 1998

The absorption cross sections of HOI have been obtained at room temperature between 280 and 490 nm. HOI was generated in situ by laser photolytic production of OH in the presence of I_2 and its absorption of UV−visible light measured using both a gated diode array camera and at several wavelengths by a photomultiplier. Calibration was performed relative to I_2 loss. The absorption spectrum consists of two unstructured bands with maxima at 340.4 nm ($\sigma_{max} = (3.85 \pm 0.4) \times 10^{-19}$ cm^2) and 406.4 nm ($\sigma_{max} = (3.30 \pm 0.3) \times 10^{-19}$ cm^2) and is approximated closely by a semilogarithmic two-band Gaussian function. The cross section data were used to calculate an HOI lifetime with respect to photodissociation in the troposphere of between 170 and 100 s for solar zenith angles of 70° and 30°, respectively. The photolysis of HOI was investigated at 355 nm and was found to generate OH radicals with a quantum yield close to unity.

1. Introduction

Iodine chemistry has been considered for almost two decades to play a role in tropospheric ozone depletion[1−5] and has recently been incorporated in modeling stratospheric[6] ozone loss. Solomon et al.[6] have reviewed global iodine sources and show that natural iodocarbons represent the major contributor to the iodine content of the atmosphere, while anthropogenic sources are thought to account for less than 10%. The most investigated of this group of compounds is CH_3I, which is produced by marine algae.[1] Boundary-layer concentrations of CH_3I typically range between 1 and 4 pptv, although concentrations as high as 43 pptv have been reported[7] for marine regions of high biogenic activity. Recently, marine sources of other iodocarbons such as CH_2I_2, C_2H_5I, and CH_2ICl have been identified,[8] which may be of a greater combined source strength than that of CH_3I, and as suggested by the Arctic measurements of Schall and Heumann,[9] CH_3I may only account for 26% of marine iodine released to the atmosphere.

The production of reactive iodine from iodocarbons (RI below) occurs mainly via rapid photodissociation in the troposphere:

$$RI + h\nu \rightarrow R + I \qquad (1)$$

A globally averaged lifetime of about 4 days has been calculated[6] for CH_3I, although the lifetime for CH_2I_2, for example, will be considerably reduced from this value because of the greatly increased overlap of the solar flux and its UV absorption spectrum.[10]

The reaction of I atoms with O_3 is part of a catalytic ozone-destroying cycle:

$$I + O_3 \rightarrow IO + O_2 \qquad (2)$$

$$IO + HO_2 \rightarrow HOI + O_2 \qquad (3)$$

$$HOI + h\nu \rightarrow I + OH \qquad (4a)$$

$$\text{(net)} \qquad HO_2 + O_3 \rightarrow OH + 2O_2$$

In a modeling study of the effect of iodine on tropospheric chemistry Davis et al.[3] found that this cycle could contribute significantly to ozone loss in the lower troposphere and also showed that HOI is the dominant tropospheric iodine-containing species at altitudes below 8 km.

Recently, Solomon et al.[6] proposed that iodine chemistry may contribute to the negative trends in ozone concentrations that have been observed in the past few decades in the lower stratosphere. Since the tropospheric lifetime of iodocarbons with respect to photolysis is very short, it was suggested that transport to the stratosphere can occur only via convective processes in equatorial regions. However, recent measurements by Wennberg et al.[11] and Pundt et al.[12] indicate that there is not more than 0.2 pptv of IO in the lower stratosphere and the potential impact of iodine chemistry on stratospheric ozone remains a matter of debate. Since the efficiency of the tropospheric ozone loss cycle above is influenced by the photostability of HOI, accurate values for its absorption cross sections are required to enable the calculation of its photodissociation rate constant.

To date, only an unpublished determination of the UV−visible absorption cross sections of HOI (Jenkin[13]) is available, in which HOI was generated in the modulated photolysis of flowing H_2O_2, I_2, and N_2 mixtures:

$$H_2O_2 + h\nu\,(254\text{ nm}) \rightarrow 2OH \qquad (5)$$

$$OH + I_2 \rightarrow HOI + I \qquad (6a)$$

HOI absorption was calibrated relative to the I_2 lost. The spectrum displays two broad bands with maxima at 335 and 410 nm and cross sections of σ_{max}^{335nm} and σ_{max}^{410nm} of 2.1×10^{-19} and 2.3×10^{-19} cm^2, respectively. Jenkin[13] notes complications due to heterogeneous processes, and although the photolysis of H_2O_2 in the presence of I_2 appears to be a clean method for the in situ preparation of HOI, it suffers from problems of surface loss or possible surface reaction that is unavoidable with the long photolysis period of 3 s.

S1089-5639(98)00430-7 CCC: $15.00
Published on Web 04/08/1998

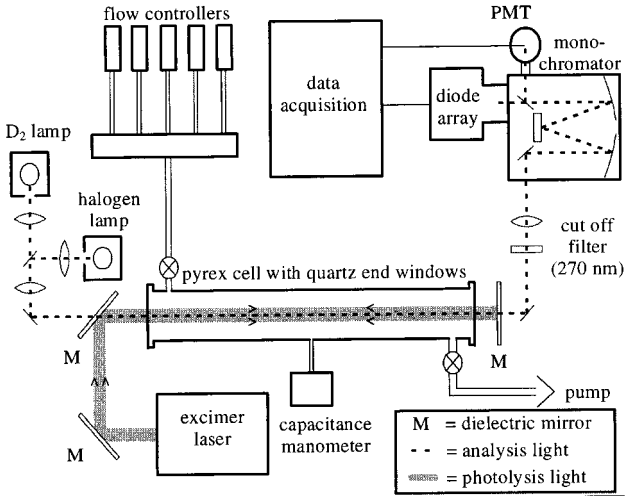

Figure 1. Schematic diagram of the experimental setup used for the absorption study.

In the work described here, the same chemical HOI generation scheme was employed, but the problem of surface reaction or loss was overcome by using pulsed laser photolysis coupled with rapid recording of the postflash absorption with a fast, gated diode array. New values for the absorption cross sections of HOI are reported at 295 K, and calculations to extrapolate this room-temperature data to atmospherically relevant temperatures are also reported.

It is generally assumed that the products of the photodissociation of HOI are OH and I, although this remains untested experimentally. Assuming an enthalpy of formation[14] for HOI of -60 ± 7 kJ mol^{-1}, the thermodynamic photodissociation thresholds for reactions 4a−4c correspond to wavelengths of 582 ± 20, 356 ± 8, and 295 ± 9 nm, respectively (heats of formation of products at 298 K taken from ref 15).

$$\mathrm{HOI} + h\nu \rightarrow \mathrm{OH} + \mathrm{I} \qquad (4a)$$

$$\rightarrow \mathrm{HI} + \mathrm{O}(^3\mathrm{P}) \qquad (4b)$$

$$\rightarrow \mathrm{IO} + \mathrm{H} \qquad (4c)$$

All reaction channels are therefore accessible over part of the wavelength range of HOI absorption (280−490 nm; see later). Reported here is the first direct observation of the OH radical from HOI photolysis and a measurement of the quantum yield at 355 nm.

2. Experimental Section

2.1. Cross Section Determination between 280 and 500 nm. The experimental apparatus used for cross section determinations is displayed in Figure 1 and has been described elsewhere,[16] though some modifications to the reaction cell are discussed. A 1.3-m cylindrical Pyrex cell of 5-cm internal diameter was equipped with quartz end-windows; a dielectric mirror enabled the photolysis beam (excimer laser, Lambda Physik LPX 300) and the probe beam (D_2 lamp) to be overlapped collinearly along the cell axis. A second dielectric mirror behind the exit window reflected the photolysis beam back through the cell, thus doubling the effective absorption path length for dissociation of H_2O_2. The collimated probe beam (single pass) sampled only a small central part of the volume swept out by the photolysis beam before being focused onto the entrance slit of a monochromator. Light from the laser was prevented from entering the monochromator by use of an appropriate filter (Schott, WG 280). The 0.5-m monochromator (grating with 150 lines mm^{-1} blazed at 500 nm, total spectral range of approximately 220 nm) was equipped with both a gated diode array detector and a photomultiplier tube (PMT). The entrance slit of the monochromator for diode array measurements was set at 0.1 mm, resulting in a resolution of 1.2 nm (fwhm of the Hg 435.8 nm line). The wavelength scale was calibrated to an accuracy of 0.3 nm with the emission lines of a low-pressure Hg lamp. For PMT measurements the entrance and exit slits of the monochromator were set at 0.25 mm, resulting in a resolution of approximately 2 nm. All experiments were performed at 295 ± 2 K with N_2 or He bath gas.

OH radicals were generated by the 248-nm photolysis of H_2O_2 (reaction 5), where the quantum yield[17] for OH production is 2. Furthermore, no detectable photolysis of I_2 occurs at this wavelength. Although the vapor pressures of H_2O_2 and I_2 and complications related to aerosol formation placed upper limits on concentration of about 1×10^{16} and 4×10^{15} cm^{-3} respectively, the room-temperature rate constants[15] $k_6 = 1.8 \times 10^{-10}$ and $k_7 = 1.7 \times 10^{-12}$ cm^3 s^{-1} ensured that over 97% of OH radicals were converted to HOI in a few microseconds via reaction 6a, with less than 3% contribution from reaction 7. Time-resolved PMT measurements confirm that there is prompt loss of I_2 and prompt formation of HOI.

$$\mathrm{H_2O_2} + h\nu\ (248\ \mathrm{nm}) \rightarrow 2\mathrm{OH} \qquad (5)$$

$$\mathrm{OH} + \mathrm{H_2O_2} \rightarrow \mathrm{HO_2} + \mathrm{H_2O} \qquad (7)$$

Diode array measurements were made over the wavelength range 280−500 nm and comprised coaddition of 500 laser pulses with light intensity recorded 50 ms before the laser pulse (I_0), and the postphotolysis spectra 60 μs after the laser pulse (I_t). The 60-μs delay after firing the laser prevented detection of fluorescence from the filter. Absorption over a time window of 5 ms was calculated by the relationship $\mathrm{abs}(t) = \ln(I_0/I_t)$.

Time-resolved absorption measurements were performed at several wavelengths with the PMT and consisted of the coaddition of 100 laser pulses. As with the diode array measurements, I_0 was obtained by averaging the PMT signal obtained before the laser pulse. I_t values were recorded for up to 4 s after the laser pulse at a resolution of between 10 μs and 1 ms. The initial absorption was obtained from the prompt, postflash PMT signals. It was possible to measure at four single wavelengths for each time-resolved experiment by scanning the monochromator between laser shots. Each experiment contained a measurement at 340 nm (maximum of first absorption band) for the purpose of normalization if there was any slight variation in reactant concentration or laser energy between measurements.

H_2O_2 was introduced into the cell by bubbling a flow of N_2 or He through a thermostated bubbler containing liquid H_2O_2. A flow of I_2 was generated by passing N_2 or He through a glass column containing iodine crystals at ambient temperature. All gas flows were regulated by mass flow meters, and the in situ concentrations of reactants were determined by absorption measurements at 220 nm for H_2O_2 ($\sigma = 2.58 \times 10^{-19}$ cm^2) [15] and at 500 nm for I_2 ($\sigma = 2.19 \times 10^{-18}$ cm^2).[18] With a total pressure of 70−100 Torr and flow rates between 2000 and 3000 cm^3 (STD) min^{-1} (sccm), the residence time in the cell was about 5 s. The time between the laser pulses was always at least a factor 2 greater than the residence time, thus ensuring that the photolysis products were removed prior to the next pulse.

For calibration of the HOI cross section, an absolute value of the iodine cross section was required at 436 nm (see later)

and was measured in the present study at the same resolution as the diode array measurements and in the same reaction cell. Prior to its admission to the cell, the iodine was subjected to several freeze/pump/thaw cycles to ensure that all residual gas was removed. The I_2 pressure in the absorption cell was measured with an accuracy of 1%.

The stated purities of I_2, N_2, and He were 99.8% (Aldrich), 99.999% (Linde), and 99.999% (Linde), respectively. The H_2O_2 (80 wt %) was supplied by Solvay Interox and was concentrated to >90 wt % by passing helium through the liquid for several days prior to use.

2.2. Photolysis of HOI at 355 nm: Detection of OH. By analogy to HOBr[19] and HOCl,[20−22] the expected products upon photolysis of HOI in its UV−visible absorption bands are OH and I atoms:

$$\mathrm{HOI} + h\nu \rightarrow \mathrm{OH} + \mathrm{I} \qquad (4a)$$

To test this supposition and to determine the quantum yield of OH formation at 355 nm, experiments were carried out in a separate apparatus in which OH can be detected directly and sensitively. Most of the components of this setup have been recently described,[23] and only details relevant to the present experiments are given here. As in the UV−visible absorption measurements, HOI was generated from the reaction of OH with I_2. For these experiments, HNO_3 was preferred to H_2O_2 as the OH source, since its cross section at 355 nm is a factor of ∼100 lower.

$$\mathrm{HNO_3} + h\nu\ (248\ \mathrm{nm}) \rightarrow \mathrm{OH} + \mathrm{NO_2} \qquad (8)$$

Primary OH (OH^P) formed in reaction 8 was monitored by resonance fluorescence and its decay due to reaction with HNO_3 and I_2 monitored over a period of several milliseconds. A dielectric mirror enabled a second laser beam (Nd:YAG, third harmonic at 355 nm) to be coupled into the fluorescence cell on the same optical axis as the 248-nm excimer laser. Both laser beams passed through two irises of 5-mm diameter before entering the cell, and their collinearity was checked frequently using a He−Ne laser that is permanently aligned with the fluorescence cell and the lasers.

The YAG laser provided a high-intensity source for HOI dissociation in its first absorption band. The resulting signal due to secondary OH (OH^S) was also followed over a few milliseconds. The timing of the lasers was arranged so that the primary OH signal had decayed to ≤1% of its initial magnitude before the YAG laser fired (a 2.7-ms delay), ensuring optimal yield of HOI. The 355-nm laser fluences were measured by a newly calibrated joule meter (Gentec ED-100A) placed behind the Brewster exit window (93 ± 3% transmittance at 355 nm) of the photolysis cell and a colored glass filter (24 ± 2% transmittance at 355 nm). The active area of the joule meter is 4.3 mm in diameter, and it therefore sampled only the central 70% of the YAG beam. The 355-nm fluences at the center of the cell were varied between 17.1 and 121.1 mJ cm^{-2}, which convert to 3.1×10^{16} and 2.2×10^{17} photons cm^{-2}, respectively.

The concentration of HNO_3 in the photolysis cell was obtained by diode array absorption spectroscopy in a separate vessel linked serially in flow to the photolysis cell. The concentration of I_2 was calculated from the measured decay rate of OH by using the known rate coefficient for OH + I_2 at 295 K (1.8×10^{-10} cm^3 s^{-1}).[15] The concentrations of HNO_3 and I_2 were held constant at 1.6×10^{15} and 1.15×10^{13} cm^{-3}, respectively. Under these conditions, ∼90% of the primary OH reacted with I_2. The initial concentration of primary OH (from HNO_3 photolysis) was estimated from the fluorescence signal as $\sim 6 \times 10^{11}$ cm^{-3}. A total pressure of 15 Torr and a total flow rate of 103 sccm enabled the lasers to run at a 10-Hz repetition rate with the reaction volume (defined by the intersection of the emission of the microwave lamp used to excite the OH, and the laser beams) to be replenished with fresh reactants after each pulse. The stated purities of I_2 and Ar were 99.8% (Aldrich) and 99.999% (Linde), respectively. Anhydrous HNO_3(l) was distilled from a mixture of 95% H_2SO_4 and KNO_3, stored at −40 °C, and used as a ∼3% gaseous mixture in Ar.

3. Results

3.1. UV−Visible Cross Sections Measurements. *3.1.1. Experiments with N_2 as Bath Gas.* Initial experimental checks confirmed that there is no detectable photolysis of I_2 at 248 nm but revealed the presence of a small, positive, wavelength-independent postphotolysis offset corresponding to an absorption of between 5×10^{-4} and 1×10^{-3} for H_2O_2 photolysis at 248 nm with N_2 as the bath gas. Under these conditions, the fate of OH is reaction with H_2O_2 to generate HO_2 radicals (reaction 7), which do not absorb in the wavelength range of interest. The magnitude of this offset was not reproducible between consecutive experiments at fixed H_2O_2 concentrations, although it could be reduced at lower H_2O_2 concentrations. Time-resolved PMT measurements indicated that this offset persisted for around 100−150 ms and showed that in the first 5 ms (the maximum diode array gate time) it was roughly constant. There was no offset observed when only I_2 and/or N_2 were irradiated, which rules out electronic interference. The offset was also observed in experiments at atmospheric pressure both with and without the cell windows, excluding photoinduced desorption of an absorbing species. A thermal lens effect caused by the absorption of light by H_2O_2 and local heating of the bath gas was probably responsible.

The PMT measurements of the prompt absorption were shifted down by the lower limit of the offset, and an error of $\pm 5 \times 10^{-4}$ is quoted for all the following text where N_2 is indicated as the bath gas. It should be noted that this offset of 5×10^{-4} represents ∼6% of the absorption due to HOI at either of the maxima of the two bands.

In common with previous studies,[24,25] both aerosol formation and wall deposits were observed, though the latter were restricted to early experiments with high initial concentrations of H_2O_2 and I_2. Displayed in Figure 2 is an example of time-resolved measurements at selected wavelengths over a period of 0.5 s after the laser pulse. The formation of aerosol is apparent at shorter wavelengths after about 40 ms and at longer wavelengths after about 80 ms. This is consistent with the increasing size of the aerosol as a function of time and the associated scattering of the probe beam. The diode array measurement of the postflash absorption was completed after a maximum of 5.06 ms after the flash and was not affected by aerosol formation as displayed in Figure 2. Further, some "off-white" wall deposits were observed near the outlet of the cell. Samples of this deposit were stable when heated to around T > 500 K, and it is believed[24] to be I_2O_5. By adjustment of the reactant concentrations, it was possible to minimize aerosol formation to the extent that no deposits were observed during a typical experimental run. It was found that the degree of aerosol formation was sensitive to the H_2O_2 concentration, which in turn controls the final HOI and I atom concentrations. Subsequent gas-phase or heterogeneous reactions or nucleation involving these species is likely to be responsible for aerosol

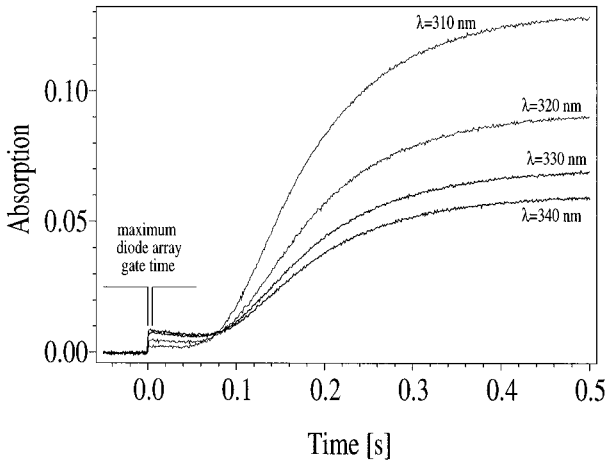

Figure 2. Examples of time-resolved absorption measurements at selected wavelengths due to HOI (prompt signal) and due to aerosol (onset at ~0.04 s for 310 nm). The diode array measurements, taken in the first 5 ms after the laser pulse, are clearly not affected by aerosol formation.

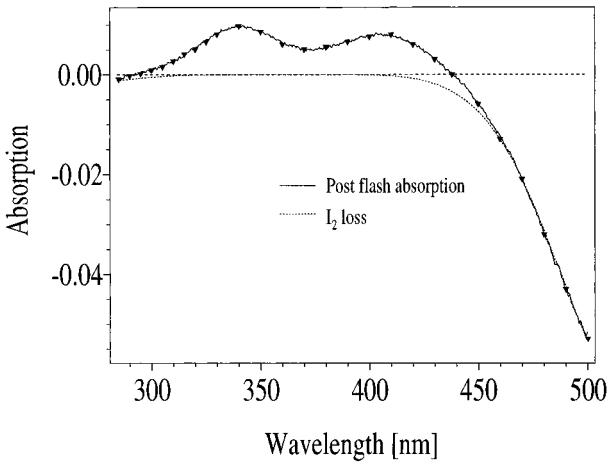

Figure 3. Postflash absorption measured with the diode array (gate time = 5 ms) over the wavelength range 280−500 nm (solid line), and the absorption due to the loss of I_2 (broken line). Also shown is the prompt absorption obtained from PMT measurements (▼) at several wavelengths. An isobestic point is found at 436 nm, where the cross sections of HOI and I_2 are equal.

formation. The concentration of H_2O_2 was reduced to 1×10^{16} cm^{-3} with I_2 maintained at $4 \times 10^{15} cm^{-3}$. Furthermore, to prevent any possible accumulation of deposits over a series of experiments, the reaction cell and windows were cleaned thoroughly by repeated washing with ethanol after each experimental run. This procedure proved vital to the measurement of a reproducible HOI spectrum and is discussed later.

Experiments were carried out with H_2O_2 and I_2 concentrations varied in the range $(0.5-1.0) \times 10^{16}$ and $(2-4) \times 10^{15}$ cm^{-3}, respectively, and laser-pulse energies were varied by a factor of 3. A typical postflash absorption measurement made with the diode array (gate time = 0.06−5.06 ms after the laser pulse) in the wavelength range 280−500 nm is displayed in Figure 3, together with the I_2 reference spectrum (measured as part of this work), which was scaled to fit the postflash absorption at 500 nm and used for preliminary spectral subtraction. Also shown are the initial absorptions obtained from the prompt PMT signals at selected wavelengths. Below 330 nm and above 436 nm there is negative contribution to absorption due to the loss of I_2. Below 350 nm the small negative contribution to absorption due to the loss of H_2O_2 was calculated from the measured loss of I_2 and the cross sections[15] for H_2O_2 and accounted for a maximum absorption of $\sim 2.6 \times 10^{-4}$ at 280 nm. To account for the offset described earlier, it was necessary to perform several iterations of a fitting procedure, which is now described.

Initially, the postflash absorption spectrum was shifted down by 5×10^{-4} absorption units. The absorption due to I_2 loss (determined by fitting the I_2 reference spectrum onto the postflash absorption at 500 nm) and the calculated absorption due to H_2O_2 loss were subtracted. The resulting HOI absorption spectrum was fitted with a semilogarithmic Gaussian function (eq i) for each of the two bands, and the quality of the fit was calculated:

$$\text{absorption}\ (\lambda) = \text{abs}_{\text{max}} \exp\left\{-\text{FW}\left[\ln \frac{\lambda_{\text{max}}}{\lambda}\right]^2\right\} \qquad \text{(i)}$$

where abs_{max} and λ_{max} are the absorption and wavelength at the peak of each band and FW is a width parameter. To improve the quality of the fit, it was then possible to shift the postflash spectrum up or down by up to 5×10^{-4} absorption units. The absorption due to I_2 loss was again fitted at 500 nm and subtracted together with the absorption due to H_2O_2 loss, and the HOI spectrum was fitted again. This procedure was repeated until the best possible fit was achieved. The overall shift in the postphotolysis spectrum never exceeded the upper limit of the offset (1×10^{-3} absorption units). At 436 nm the absorption due to HOI formation is exactly canceled by that due to I_2 removal (isobestic point), and since there is no possible contribution to absorption by H_2O_2 loss at this wavelength, the cross section of HOI can be equated to that of I_2, since a 1:1 conversion of I_2 to HOI is considered to occur. As expected, at the isobestic point, no change in absorption was observed in PMT experiments at 436 nm, as shown in Figure 3. The validity of this approach, which not only provides a method of relative calibration of the HOI cross section but also serves as a test of experimental reproducibility, is discussed shortly.

The variation of the diode array gate times over the ranges 60−560 μs and 60−5060 μs resulted in no change in the position of the isobestic point or the form of the spectrum. As confirmed in Figure 3, there is good agreement between the diode array and prompt PMT measurements, which provides evidence that the diode array measurements, generally made with a gate time of 0.06−5.06 ms, were not influenced by aerosol formation. Furthermore, this also demonstrated that diffusion into or out of the observation region was unimportant on this time scale under the experimental conditions employed. For repeated experiments and all variations in reactant concentrations and laser energy (by a factor of 3), both the isobestic point (436 ± 0.5 nm) and the form of the spectrum were reproducible within the noise level. This reproducibility underlines the reliability of the method used to account for the offset described above.

3.1.2. Experiments with He as Bath Gas. When N_2 was replaced by He, the postphotolysis offset was removed completely. This may be due to the better thermal conductivity of He compared with that of N_2 and to the elimination of the thermal lens effect.

The final experiments described in the section above were repeated under the same conditions and with the same procedure but with the N_2 bath gas replaced with He. The method used to subtract the contribution to postflash absorption due to loss of absorbing reactants was as above, except that no shifting or fitting of the postflash absorption was required. For all variations in reactant concentration and laser energy, both the form of the spectrum and the isobestic point (436 ± 0.5 nm)

TABLE 1: Parameters Obtained from the Gaussian Fit to the HOI Cross Sections at 295 and 0 K in He

band	λ_{max} [nm]	FW[a]	$10^{19}\sigma_{max}$[a] [cm^2]	FW[b]	$10^{19}\sigma$[b] [cm^2]
1st	340.4	162.8	3.85	183.8	4.09
2nd	406.4	170.2	3.30	192.1	3.51

[a] At 295 K. [b] At 0 K. The parameters calculated at 0 K allow the prediction of the cross sections at any temperature (see text) by use of the equation $\sigma(\lambda, T) = \sigma^{1st}_{max}(T) \exp\{-FW^{1st}(T)[\ln(\lambda^{1st}_{max}/\lambda)]^2\} + \sigma^{2nd}_{max}(T) \exp\{-FW^{2nd}(T)[\ln(\lambda^{2nd}_{max}/\lambda]^2\}$ where $\sigma_{max}(T) = \sigma_{max}(0)(\tanh)^{1/2}$, FW($T$) = FW(0) tanh, and tanh = tanh[$hc_0\omega_e/(2kT)$].

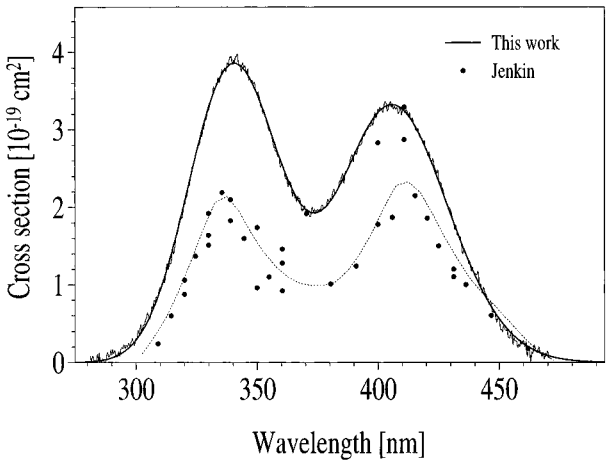

Figure 4. Averaged absorption cross section measurements at 295 K (noisy line) together with a two-band Gaussian fit. Also shown are the data of Jenkin[13] (●). The broken line is the fit given by Jenkin.

were reproducible within the noise level and are in excellent agreement with the results obtained in N_2.

3.1.3. Cross Section Calibration. The cross sections of I_2 were measured in the wavelength range 280−510 nm. At 436 nm a value of $(1.41 \pm 0.05) \times 10^{-19}$ cm^2 was obtained and was used to calibrate the HOI spectrum. A value of $(2.25 \pm 0.09) \times 10^{-18}$ cm^2 was obtained at 500 nm, which is in good agreement with the value of 2.19×10^{-18} cm^2 given by Tellinghuisen.[18] In common with previous determinations, the absorption due to I_2 above 500 nm did not scale linearly with concentration, precluding the reliable measurement of any possible absorption due to HOI at $\lambda > 500$ nm. The absorption cross sections of HOI measured in the He bath gas were fitted with the semilogarithmic Gaussian function shown below for each absorption band:

$$\sigma(\lambda) = \sigma_{max}(T) \exp\left\{-FW(T)\left[\ln \frac{\lambda_{max}}{\lambda}\right]^2\right\} \qquad \text{(ii)}$$

where $\sigma_{max}(T) = \sigma_{max}(0)(\tanh)^{1/2}$, FW($T$) = FW(0) tanh, and tanh = tanh[$hc_0\omega_e/(2kT)$]. The value of the cross section and wavelength at the maximum absorption $\sigma_{max}(T)$ and λ_{max}, and the width parameter FW(T) are obtained by fitting eq ii to the 295 K absorption cross sections. Since the harmonic vibrational wavenumber $\omega_e \approx 575$ cm^{-1} is known[25,26] for the I−O stretch in HOI, values of $\sigma_{max}(0)$ and FW(0), which are the corresponding parameters at 0 K, can be calculated. This semiempirical treatment allows the prediction of the HOI absorption cross sections at any temperature. Table 1 shows the best-fit parameters at 295 K and the corresponding parameters calculated for 0 K. The two absorption bands are centered at 340.4 and 406.4 nm, with cross sections of $(3.85 \pm 0.4) \times 10^{-19}$ and $(3.30 \pm 0.3) \times 10^{-19}$ cm^2, respectively, at 295 K. Figure 4 displays the fit to the averaged absorption cross sections at 295 K and compares this new data with the previous determination.[13] The λ_{max} of Jenkin[13] are at 335 and 410 nm, in good agreement with the present data, although the cross sections are a factor of about 1.8 (first band) and 1.4 (second band) lower. The uncertainty in the present cross sections is estimated to be ±10% based upon the respective errors in the isobestic point, the measured I_2 cross section at 436 nm, and I-atom recombination (see Discussion). Table 2 shows the absorption cross sections obtained from the best Gaussian fit to the 295 K data, which are given at 5-nm intervals.

TABLE 2: HOI Absorption Cross Sections at 295 K

λ [nm]	σ [10^{-19} cm^{-2}]	λ [nm]	σ [10^{-19} cm^{-2}]
280	0.0077	390	2.66
285	0.0226	395	2.98
290	0.0589	400	3.22
295	0.137	405	3.32
300	0.286	410	3.27
305	0.541	415	3.07
310	0.926	420	2.75
315	1.45	425	2.35
320	2.07	430	1.92
325	2.72	435	1.50
330	3.29	440	1.13
335	3.70	445	0.813
340	3.85	450	0.563
345	3.77	455	0.376
350	3.47	460	0.242
355	3.04	465	0.150
360	2.58	470	0.0904
365	2.21	475	0.0525
370	1.98	480	0.0296
375	1.94	485	0.0161
380	2.07	490	0.0086
385	2.33		

3.2. Photolysis of HOI at 355 nm (and 532 nm). Figure 5 shows time-dependent OH profiles following the 248-nm laser pulse at $t = 1000$ μs (primary OH radical generation, OH^P) and secondary OH (OH^S) formation due to HOI photolysis following the 355-nm pulse at $t \approx 3700$ μs.

$$HNO_3 + h\nu\ (248\ nm) \rightarrow OH^P + NO_2 \qquad (8)$$

$$OH^P + I_2 \rightarrow HOI + I \qquad (6a)$$

$$HOI + h\nu\ (355\ nm) \rightarrow OH^S + I \qquad (4a)$$

To be sure that the secondary OH signal was from HOI photolysis, experiments were carried out in which the excimer laser was not triggered (i.e., no primary OH formation) and in which either the HNO_3 or the I_2 was not present. In all cases, HOI formation is precluded and secondary OH was not observed. This rules out that any product of the 248-nm photolysis of HNO_3, and its subsequent photolysis at 355 nm (e.g., HONO), is the source of OH^S or that HNO_3 is photolyzed at 355 nm to directly yield OH. Experiments in which the firing sequence of the lasers was reversed (i.e., 355 nm before 248 nm) yielded no 355-nm-induced OH signal (OH^S), confirming that the formation of OH^S requires conversion of OH^P to HOI from the directly preceding 248-nm photolysis of HNO_3 and is not due to buildup of any product that was still present in the cell after 0.1 s (the delay between pairs of laser pulses).

It can be shown that the relative initial signal height (obtained by extrapolation to the time of the respective laser pulses) of the primary and secondary OH signals (OH^P_0 and OH^S_0, respectively) depends only upon the fluence of the 355-nm laser pulse, on the cross section of HOI, and the quantum yield of OH

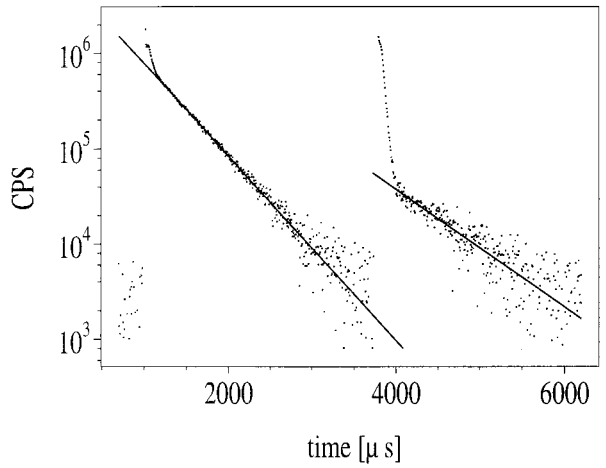

Figure 5. Primary and secondary OH (OH^P and OH^S) formed in the 248-nm photolysis of HNO_3 and the 355-nm photolysis of HOI, respectively. The excimer laser (248 nm) was triggered at $t = 1000$ μs to produce OH^P, the YAG laser (355 nm) at 3670 μs to make OH^S. The strong, rapidly decaying signals directly after the laser pulses are due to optical and electrical interferences and are ignored in the analysis. CPS = counts per second.

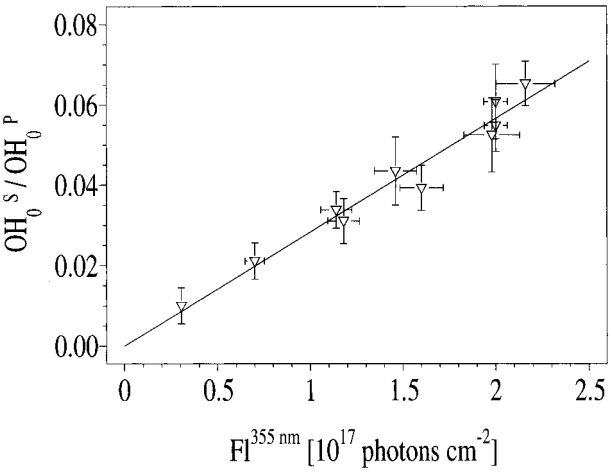

Figure 6. Plot of the ratio OH_0^S/OH_0^P vs laser fluence (Fl) at 355 nm. The slope of the fitted line through the data is equal to the product of the quantum yield of OH formation and the cross section of HOI at 355 nm and is $(2.83 \pm 0.19) \times 10^{-19}$ cm^2.

formation at 355 nm. Assuming 100% conversion of OH^P to HOI, the ratio of OH_0 signals is given by

$$\frac{OH_0^S}{OH_0^P} = Fl^{355nm}\sigma_{355nm}^{HOI}\Phi_{355nm}^{HOI} \qquad \text{(iii)}$$

where Fl^{355nm} is the average fluence at 355 nm through the reaction volume (in photons cm^{-2}), σ_{335nm}^{HOI} is the absorption cross section of HOI (cm^2) at 355 nm, and Φ_{335nm}^{HOI} is the quantum yield of OH formation at this wavelength.

According to eq iii, a plot of $(OH_0^S/OH_0^P$ versus Fl^{355nm} should yield a straight line with a slope equal to the product of the cross section and quantum yield of OH at 355 nm. Such a plot is displayed in Figure 6 and has a slope of $\sigma_{355nm}^{HOI}\,\Phi_{355nm}^{HOI} = (2.83 \pm 0.19) \times 10^{-19}$ cm^2.

As stated above, eq iii is valid for the assumption of 100% conversion of OH^P to HOI, which, as discussed in the Experimental Section, was not the case, since some OH^P reacts with the HNO_3 precursor. In addition, observations of OH decays in the absence of reaction partners (from experiments in which N_2O/H_2O were used as 193-nm photolytic precursors of OH), and calculations using the diffusion coefficient of OH at 15 Torr Ar show that some are also lost through diffusion out of the reaction/detection zone in the ~2.5-ms period between laser pulses, typically at a rate of 100 ± 50 s^{-1}. We calculate that a total of $13 \pm 2\%$ is lost (does not form HOI) and correct our result to $\sigma_{355nm}^{HOI}\,\Phi_{355nm}^{HOI} = (3.20 \pm 0.25) \times 10^{-19}$ cm^2 to take this into account. If we now take the 355-nm cross section of HOI determined in the absorption study ($\sigma_{355nm}^{HOI} = \{3.04 \pm 0.3\} \times 10^{-19}$ cm^2), we can derive a quantum yield of OH formation as $\Phi_{355nm}^{HOI} = 1.05 \pm 0.13$. The errors reflect the combined uncertainties of the weighted fit (95% confidence) in Figure 6 where the error bars on the *x* axis (fluence) are based on observations of reproducibility. The errors in relative OH signal are 95% confidence limits from the exponential fits to the OH decays.

There are also potential systematic errors related to the overlap of the YAG laser beam, which has a clipped Gaussian intensity distribution, and the microwave lamp emission. Efforts were made to ensure that the laser beams were coaxial through the cell and that the OH signal was maximized by adjusting the microwave lamp emission to overlap with these beams at the focal point of the telescopic detection optics. Under these conditions, it can be shown that if the volume resulting from the overlap of the microwave emission and YAG laser beam is of uniform intensity and has a projected area that is the same as or greater than the area of the joule meter (~4-mm diameter), no error is incurred. However, since the intensity distribution of the microwave lamp is unknown and the projected area of intersection may be smaller than 4 mm, a possible underestimation of the fluence at the center of the cell, and therefore an overestimation of the quantum yield, may occur. We therefore prefer to quote the final result as $\Phi_{355nm}^{HOI} = 1.05_{-0.34}^{+0.13}$.

Experiments were also carried out using the second harmonic of the YAG at 532 nm and identical conditions to those outlined above. Despite the use of very high fluences (1×10^{18} photons cm^{-2}), no secondary OH was formed, indicating either that HOI does not absorb at 532 nm or that the quantum yield is zero. Since the thermodynamic threshold for dissociation to OH + I corresponds to a wavelength of 582 ± 20 nm, the first explanation seems most likely and enables us to set an upper limit of $\sim 1 \times 10^{-20}$ cm^2 for σ (HOI) at 532 nm.

4. Discussion

4.1. HOI Cross Sections. The highly reproducible isobestic point and form of the spectrum with variation of laser energy, bath gas, and the initial concentrations of H_2O_2 and I_2, and the excellent agreement between the diode array and PMT measurements of the cross sections, provide strong evidence for the validity of the results presented here. However, the UV−visible cross sections determined in this work are considerably higher than those reported by Jenkin[13] despite the use of the same gas-phase chemical scheme for the generation of HOI and the same method for calibration. In the following section a number of potential systematic errors from which both systems may suffer are evaluated.

Since the calibration is performed by measuring postflash I_2 loss, it is necessary to consider any reactions that could falsify this procedure. One reaction is the recombination of I atoms to re-form I_2:

$$I + I + M \rightarrow I_2 + M \qquad (9)$$

From the expression given by Jenkin et al.[27] for the pressure-dependent rate constant for reaction 9 where M = N_2 at 295 K,

an effective bimolecular rate constant of $k_9 = 2.3 \times 10^{-14}$ cm^3 s^{-1} is calculated at 70 Torr total pressure. The maximum initial concentration of I atoms in the present study was approximately 2×10^{14} cm^{-3}, and re-formation of I_2 is calculated to be too slow to be significant. This was confirmed by time-resolved PMT measurements in which no recombination of I atoms was detected in the first 5 ms after the laser pulse.

As shown by Vaghjiani and Ravishankara,[17] the quantum yields for OH, O(^{3}P + ^{1}D), and H(^{1}S) from H_2O_2 photolysis are 2.09 ± 0.36, <0.002, and <0.0002, respectively. This established that the quantum yield for OH production is 2 and more importantly that the yields of O and H atoms, which react rapidly with I_2, are negligible. O(^{3}P) atoms are also formed in the self-reaction of OH (12):

$$O(^3P) + I_2 \rightarrow IO + I \quad (10)$$

$$H + I_2 \rightarrow HI + I \quad (11)$$

$$OH + OH \rightarrow H_2O + O \quad (12)$$

The formation of O(^{3}P) atoms (and any resultant loss of I_2) could be ruled out in the present experiments, since the IO product of the reaction 10 was not observed, despite the large absorption cross sections of IO and correspondingly low detection limits.

An assumption inherent to the present method of calibration is that each I_2 lost generates one HOI. The almost exclusive formation of HOI via reaction 6a was determined by Loewenstein and Anderson[28] who give an upper limit to the ratio (k_{6b}/k_6) of 0.01 at 298 K.

$$OH + I_2 \rightarrow IO + HI \quad (6b)$$

Barnes et al.[25] employed reaction 6a to produce HOI and found no evidence for the formation of HI in the product IR spectrum. Also, in the present study there is no evidence for the other product, IO (see above). Since it is clear that HOI is the exclusive product from reaction 6 at ambient temperatures, the validity of the HOI cross section calibration technique described earlier is given, in that a 1:1 conversion of I_2 to HOI occurs.

The experimental conditions employed ensured that over 97% of the OH radicals were consumed by I_2, the remainder reacting with H_2O_2 via reaction 7 to form HO_2 and H_2O, neither of which absorb strongly in the wavelength region of interest.

As mentioned earlier, it was necessary to clean the cell and windows after each experiment to obtain reproducible HOI spectra. When this was not done, the magnitude of the second band was observed to increase progressively until it became around 20% larger than the first. In these experiments, "off-white" deposits were observed on the cell walls and to a much lesser extent on the windows. It is not clear whether these deposits are the site of heterogeneous reaction, which forms a product or products that may enter the gas phase and contaminate the measurement, or whether the small buildup on the windows affects the form of the spectrum.

In the previous determination by Jenkin,[13] it was noted that during the course of a measurement, the initial absorption was low but increased with time until a reasonable degree of reproducibility was achieved. The cross section data obtained in the present study are compared with that of Jenkin in Figure 4. The second band in the Jenkin data is slightly higher than the first, which may be related to the presence of deposits as described above, and the degree of scatter around the second band in the Jenkin data suggests poor reproducibility at these wavelengths. Jenkin also reported that the loss rate of I_2 was greater than expected on the basis of reaction 6 only, which was probably due to photolysis of I_2. This would of course tend to lower the calculated cross sections of HOI as the stoichiometry of conversion of I_2 to HOI is reduced.

As shown in Figure 4, there is an excellent fit to the absorption cross sections by eq ii, which indicates the reliability of the form of the HOI spectrum reported here. A theoretical justification of the use of semilogarithmic Gaussian functions to describe the shape and temperature dependence of UV absorption continua has recently been given.[29] Equation ii has been used successfully to describe the shapes and predict the temperature dependencies of the absorption continua of the diatomic molecules Cl_2,[30] Br_2,[31] and BrCl.[31] In recent work,[32] eq ii has been shown to predict well the shape and temperature dependence of the UV spectra of methyl- and ethylperoxy radicals by treating them as quasi-diatomic species, whereby the O−O stretching frequency approximates the photoexcitation coordinate. By analogy with these peroxy radicals, in the context of electronic excitation, HOI should approximate a quasi-diatomic species. Equation ii predicts a limited temperature dependence of the absorption cross sections for HOI, with an increase of ∼5% in the maxima of both absorption bands at 220 K when compared with that at 295 K.

4.2. Photolysis of HOI at 355 and 532 nm. The photolysis of HOI at 355 nm results in OH formation with a quantum yield close to unity. This result may be expected given the continuous nature of the absorption spectrum that indicates dissociative upper electronic states between 280 and 490 nm. Similar results have been obtained for the chlorine and bromine analogues HOCl[20,22] and HOBr.[19]

The existence of a third absorption band for HOBr centered around 440 nm was detected in a photofragment study by Barnes et al.[33] and has recently been confirmed in this laboratory.[34] This band is thought to be due to excitation to a triplet state in HOBr, and this view is supported by an ab initio calculation by Francisco et al.[35] By analogy with HOBr, it may be expected that HOI should exhibit a transition to a triplet state at wavelengths above 500 nm. However, in the present cross section determination a reliable measurement of any absorption due to HOI above 500 nm was not possible owing to a nonlinearity in I_2 absorption. The photolysis of HOI and detection of OH therefore provided an alternative means to test for a dissociative absorption at 532 nm. No OH formation was found, and we conclude either that a third absorption band for HOI is considerably reduced in intensity when compared with that for HOBr or that HOI is nondissociative (dissociation via reactions 4b and 4c is not possible at 532 nm). In both cases, the atmospheric dissociation rate of HOI can be accurately calculated using the two strong absorption bands between 280 and 490 nm.

4.3. *J* Values. To calculate the atmospheric photolysis rate constant (*J* value) for HOI, a quantum yield of unity throughout the absorption region was assumed and the integral

$$J_{HOI} = \int_{280nm}^{490nm} \sigma_{HOI}(\lambda) F_{act}(\lambda)\, d\lambda \quad (iv)$$

was evaluated. The actinic flux $F_{act}(\lambda)$ is calculated with the radiative-transfer model DISORT,[36] and for large solar zenith angles the spherical geometry of the atmosphere is taken into account by employing the air-mass factor correction of Kasten and Young.[37] A more detailed description of the *J* value calculations can be found in Landgraf and Crutzen.[38] The

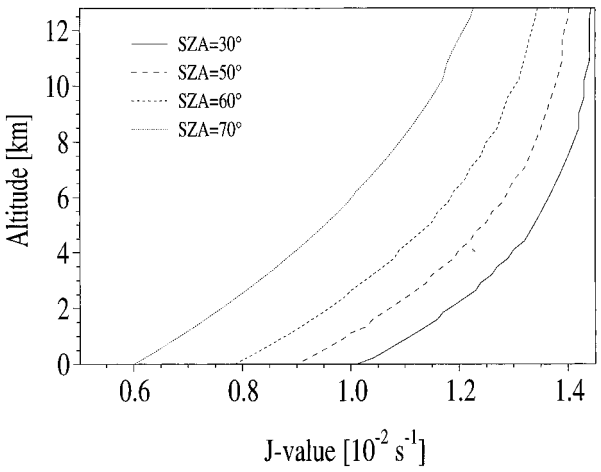

Figure 7. *J* values of HOI as a function of solar zenith angle (SZA) and altitude. An O_3 column of 300 Dobson units was used.

calculations (see Figure 7) show that the atmospheric lifetime of HOI with respect to photodissociation is very short indeed. The strong absorption bands between 350 and 490 nm overlap efficiently with the actinic flux, which is intense and has a relatively weak wavelength dependence in this range. *J* values are greater than 6×10^{-3} s^{-1} throughout most of the atmosphere, corresponding to a lifetime of less than 3 min and highlighting the fact that HOI cannot be considered a stable reservoir of iodine under sunlit conditions. The *J* values presented here are based on UV−visible absorption cross sections that are between 1.5 and 1.8 times as large as those presented in the one previous measurement (see Figure 4). Since the relative shape of the spectra are similar, previous photochemical models including HOI chemistry have therefore overestimated the lifetime of HOI by a similar factor.

5. Conclusions

New absorption cross sections for HOI have been obtained at 295 K over the wavelength range 280−490 nm. Two continuous absorption bands are observed with λ(max) at 340.4 nm, where $\sigma = (3.85 \pm 0.4) \times 10^{-19}$ cm^2, and at 406.4 nm, where $\sigma = (3.30 \pm 0.3) \times 10^{-19}$ cm^2. The quantum yield for OH formation from HOI at 355 nm was found to be close to unity. *J*-value calculations using the new absorption cross sections and quantum yield give tropospheric lifetimes of 170 and 100 s close to the surface at solar zenith angles of 70° and 30°, respectively.

Acknowledgment. Thanks are extended to J. Landgraf for the *J*-value calculations and to R. A. Cox for providing the data from the Ph.D. thesis of M. E. Jenkin. This work was supported by the Commission of the European Community ("LEXIS", Project ENV4-CT95-0013).

References and Notes

(1) Chameides, W. L.; Davis, D. *J. Geophys. Res.* **1980**, *85*, 7383.
(2) Chatfield, R. B.; Crutzen, P. J. *J. Geophys. Res.* **1990**, *95*, 22319.
(3) Davis, D.; Crawford, J.; Liu, S.; McKeen, S.; Bandy, A.; Thornton, D.; Rowland, F.; Blake, D. *J. Geophys. Res.* **1996**, *101*, 2135.
(4) Jenkin, M. E.; Cox, R. A.; Caneland, D. E. *J. Atmos. Chem.* **1985**, *2*, 359.
(5) Jenkin, M. E. *NATO ASI Ser.* **1993**, *I7*, 405.
(6) Solomon, S.; Garcia, R. R.; Ravishankara, A. R. *J. Geophys. Res.* **1994**, *99*, 20491.
(7) Oram, D. E.; Penkett, S. A. *Atmos. Environ.* **1994**, *28*, 1159.
(8) Yokouchi, Y.; Mukai, H.; Yamamoto, H.; Otsuki, A.; Saitoh, C.; Nojiri, Y. *J. Geophys. Res.* **1997**, *102*, 8805.
(9) Schall, C.; Heumann, K. G. *Fresenius J. Anal. Chem.* **1993**, *346*, 717.
(10) Roehl, C. M.; Burkholder, J. B.; Moortgat, G. K.; Ravishankara, A. R.; Crutzen, P. J. *J. Geophys. Res.* **1997**, *102*, 12829.
(11) Wennberg, P. O.; Brault, J. W.; Hanisco, T. F.; Salawich, R. J.; Mount, G. H. *J. Geophys. Res.* **1997**, *102*, 8887.
(12) Pundt, I.; Pommereau, J. P.; Phillips, C.; Lateltin, E. *J. Atmos. Chem.*, in press.
(13) Jenkin, M. E. Ph.D. Thesis, University of East Anglia, U.K., 1991. The raw data cited in this thesis were kindly provided by R. A. Cox, M. E. Jenkin's Ph.D. supervisor.
(14) Hassanzadeh, P.; Irikura, K. K. *J. Chem. Phys. A* **1997**, *101*, 1580.
(15) DeMore, W. B.; Sander, S. P.; Golden, D. M.; Hampson, R. F.; Kurylo, M. J.; Howard, C. J.; Ravishankara, A. R.; Kolb, C. E.; Molina, M. *J. Chemical Kinetics and Photochemical data for use in stratospheric modelling*. JPL Publication 97-4; Jet Propulsion Laboratory: Pasadena, CA, 1997.
(16) Roehl, C. M.; Bauer, D.; Moortgat, G. K. *J. Phys. Chem.* **1996**, *100*, 4038.
(17) Vaghjiani, G. L.; Ravishankara, A. R. *J. Phys. Chem.* **1990**, *92*, 996.
(18) Tellinghuisen, J. *J. Chem. Phys.* **1973**, *58*, 2821.
(19) Benter, T.; Feldman, C.; Kirchner, U.; Schmidt, M.; Schmidt, S.; Schindler, R. N. *Ber. Bunsen-Ges. Phys. Chem.* **1995**, *99*, 1144.
(20) Molina, M. J.; Ishiwata, T.; Molina, L. T. *J. Phys. Chem.* **1980**, *84*, 821.
(21) Butler, P. J. D.; Phillips, L. F. *J. Phys. Chem.* **1983**, *87*, 183.
(22) Vogt, R.; Schindler, R. N. *J. Photochem. Photobiol. A* **1992**, *66*, 133.
(23) Crowley, J. N.; Carl, S. A. *J. Phys. Chem. A* **1997**, *101*, 4178.
(24) Wayne, R. P.; Poulet, G.; Biggs, P.; Burrows, J. P.; Cox, R. A.; Crutzen, P. J.; Hayman, D. G.; Jenkin, M. E.; Le Bras, G.; Moortgat, G. K.; Platt, U.; Schindler, R. N. *Atmos. Environ.* **1995**, *29*, 2677.
(25) Barnes, I.; Becker, K. H.; Starcke, J. *Chem. Phys. Lett.* **1992**, *196*, 578.
(26) Walker, N.; Tevault, D. E.; Smardzewski, R. R. *J. Chem. Phys.* **1978**, *69*, 564.
(27) Jenkin, M. E.; Cox, R. A.; Mellouki, A.; Le Bras, G.; Poulet, G. *J. Phys. Chem.* **1990**, *94*, 2927.
(28) Loewenstein, L. M.; Anderson, J. G. *J. Chem. Phys.* **1985**, *89*, 5371.
(29) Maric, D.; Burrows, J. P. *J. Chem. Phys.* **1996**, *100*, 8645.
(30) Maric, D.; Burrows, J. P.; Meller, R.; Moortgat, G. K. *J. Photochem. Photobiol. A* **1993**, *70*, 205.
(31) Maric, D.; Burrows, J. P.; Moortgat, G. K. *J. Photochem. Photobiol. A* **1994**, *83*, 179.
(32) Maric, D.; Crowley, J. N.; Burrows, *J. Phys. Chem. A* **1997**, *101*, 2561.
(33) Barnes, R. J.; Lock, M.; Coleman, J.; Sinha, A. *J. Phys. Chem.* **1996**, *100*, 453.
(34) Ingham, T.; Bauer, D.; Landgraf, J.; Crowley, J. N. *J. Phys. Chem.*, in press.
(35) Francisco, J. S.; Hand, M. R.; Williams, I. H. *J. Phys. Chem.* **1996**, *100*, 9250.
(36) Stamnes, K.; Tsay, S.-C.; Wiscombe, W.; Jayaweera, K. *Appl. Opt.* **1988**, *27*, 2502.
(37) Kasten, F.; Young, A. T. *Appl. Opt.* **1989**, *28*, 4735.
(38) Landgraf, J.; Crutzen, P. J. *J. Atmos. Sci*, in press.